nature physics

Article

https://doi.org/10.1038/s41567-023-02364-1

# Quasi-crystalline order in vibrating granular matter

Received: 4 July 2023

Accepted: 29 November 2023

Published online: 19 January 2024

Check for updates

A. Plati ✉, R. Maire, E. Fayen, F. Boulogne, F. Restagno, F. Smallenburg & G. Foffi ✉

Quasi-crystals are aperiodic structures with crystallographic properties that are not compatible with that of a single unit cell. Their discovery in a metallic alloy more than four decades ago has required a full reconsideration of our definition of a crystal structure. Quasi-crystalline structures have also been discovered at much larger length scales in different microscopic systems for which the size of the elementary building blocks ranges from the nanometre to the micrometre scale. Here we report the first experimental observation of spontaneous quasi-crystalline self-assembly at the millimetre scale. This result is obtained in a fully athermal system of macroscopic spherical grains vibrating on a substrate. Starting from a liquid-like disordered phase, the grains begin to locally arrange into three types of square and triangle tile that eventually align, forming an eight-fold symmetric quasi-crystal that has been predicted in simulation but not yet experimentally observed in non-atomic systems. These results not only demonstrate an alternative route for the spontaneous assembly of quasi-crystals but are of fundamental interest for the connection between equilibrium and non-equilibrium statistical physics.

In 1982, Shechtman discovered the first alloy with a diffraction pattern for which the Bragg peaks showed a symmetry that is forbidden by crystallography in periodic solids[1]. This discovery was initially met with resistance: the existence of structures in which atoms can be arranged in spatial structures that lack long-range periodicity and still preserve sufficient long-range order to generate discrete Bragg peaks clashed with the elegant picture of crystals as consisting of a repeating unit cell. Nonetheless, eventually, materials with this property—which were called quasi-crystals (QCs)[2]—changed the way in which scientists interpret the crystal state, by disentangling the concept of order from the concept of periodicity, to the point where the very definition of crystals had to be changed to include aperiodic structures[3].

In the following years, quasi-crystalline structures have been observed in several artificial alloys[4,5] and were even discovered in a naturally occurring mineral, icosahedrite[6], of probable extraterrestrial origin[7]. More recently, QCs have also been observed at much larger length scales in a wide range of soft-matter systems[8–17], revealing promising optical properties for next-generation photonic devices[18,19]. In soft QCs[14], two fundamental questions arise: (1) understanding up to which length scales we can observe spontaneous quasi-crystalline order and (2) identifying the key dynamical and interaction properties required for a soft-matter system to form a QC. For the former, the self-assembly of QCs has been observed on length scales that are related to the nature of the elementary building blocks that range from macromolecular structures[20] and nanoparticles[10] to polymer aggregates made of micelles[12,21], passing by polymers[8,13,15,16] and thin films[17]. To the best of our knowledge, the largest soft-matter QCs found to self-assemble consisted of micrometre-sized micelles[21,22].

The second question is of a more fundamental nature and has been extensively explored using numerical simulations. In particular, simple coarse-grained models of interacting particles make it possible to simulate systems large enough to display aperiodicity and to pin down its origin, from anisotropic repulsive[23] and attractive[24] particles to simple isotropic potentials[25–27] and hard spheres[28]. Interestingly, one of the simplest systems leading to QC formation in silico is a simple two-dimensional (2D) binary mixture of non-additive hard discs undergoing equilibrium dynamics[28,29]. This proved that, under the right geometrical conditions, quasi-crystalline order can emerge

Université Paris-Saclay, CNRS, Laboratoire de Physique des Solides, Orsay, France. ✉e-mail: andrea.plati@universite-paris-saclay.fr; giuseppe.foffi@universite-paris-saclay.fr

https://doi.org/10.1038/s41567-023-02364-1

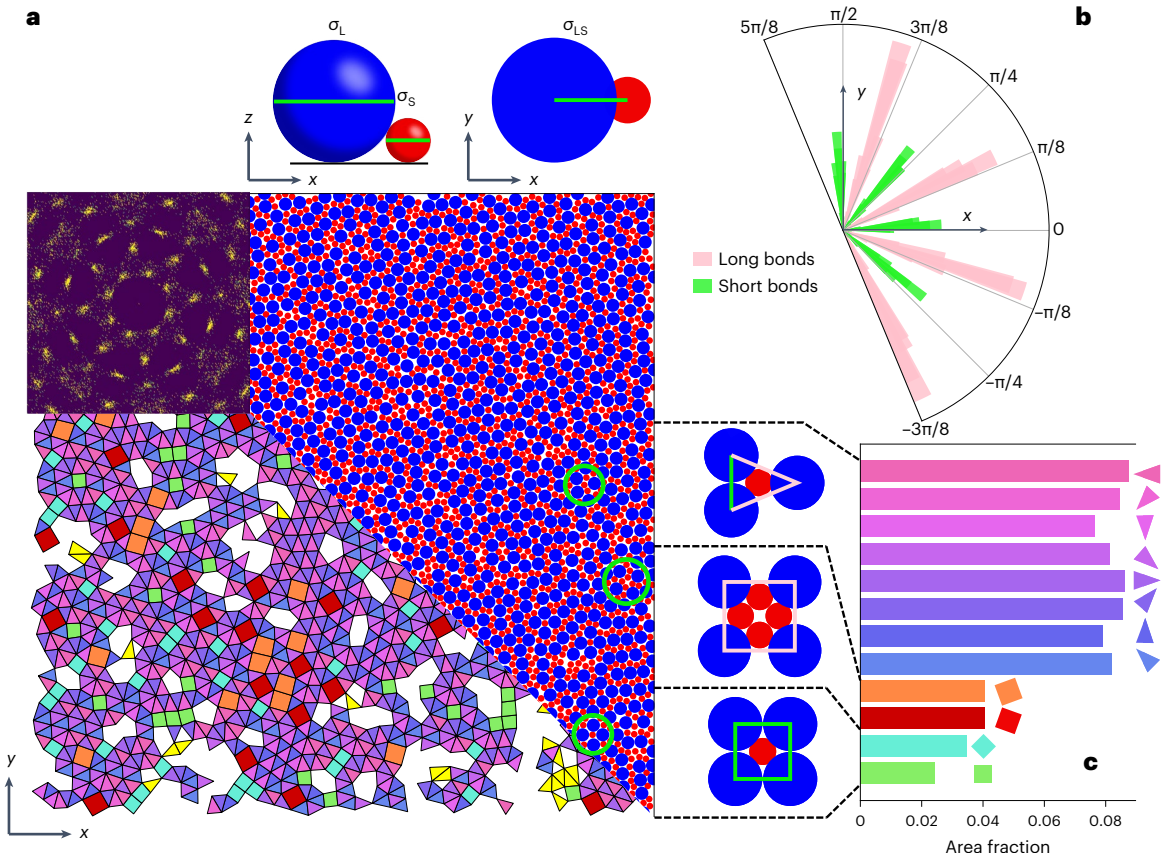


**Fig. 1 | Numerical results obtained with EDMD of a collisional model.** Here $\{q, x_S, \phi\} = \{0.5, 0.68, 0.85\}$, $N_S + N_L = 5{,}000$, $\alpha = 0.95$ and $\Delta = 0.02$, as shown in equation (1). **a**, Sketch of the granular non-additive hard-core interactions, final configuration, reconstructed tiling and structure factor. **b**, Bond orientation histogram. **c**, Histogram of the area fraction occupied by tiles of different types and orientations. The colour of the tiles is chosen according to their orientation, but we also consider defected regions that are not covered by the correct square–triangle tiling (white areas) and tiles with ambiguous orientations or misaligned with the dominant set of bond directions (yellow areas). The results are obtained with a $5.3 \times 10^{10}$-collision-long simulation. Schematic of the experimental setup (not to scale) is shown in **a**. Cropped images of a small and large grain used as a template to detect the particle position in the experimental images are shown in **b**. Each grain is identified by four light spots, each one coming from a different light panel around the setup. The larger image shows an example of particle detection with the yellow and red points that coincide with the detected positions.

from a purely entropy-driven self-assembly process. To the best of our knowledge, QC self-assembly in dissipative non-equilibrium systems where energy is constantly supplied from the environment and internally dissipated (such as active or granular matter) is still unexplored.

A natural avenue to explore QC formation beyond the colloidal scale and thermodynamic equilibrium is to use granular matter, which has proven itself to be an ideal playground for the exploration of non-equilibrium phenomena over the last three decades. Depending on how a granular system is confined and the imposed external driving, it may exhibit either a fluid-like or a solid-like behaviour[30,31] and can undergo a variety of phase transitions[32–37]. However, spontaneous QC formation in systems driven out of thermodynamic equilibrium has not yet been observed in either experiments or simulations.

In this paper, we report the experimental and numerical observation of quasi-crystalline order in a binary mixture of millimetre-sized spherical grains vibrated on a substrate. Our findings demonstrate that QCs can be formed even by macroscopic particles much beyond the scale at which thermal agitation plays a role. Our system is indeed intrinsically out of equilibrium due to dissipation arising from frictional forces and energy injection due to external driving.

In the following, we first discuss granular QC formation in the numerical simulations of a coarse-grained collisional model. We then report the main result of this paper, namely, the experimental self-assembly of a granular QC.

In both simulations and experiments, we consider a binary mixture of spherical grains ($N_S$ with diameter $\sigma_S$ and $N_L$ with diameter $\sigma_L$) lying on a horizontal substrate. To characterize the geometrical properties of such a mixture, we use the following dimensionless parameters: the size ratio $q = \sigma_S/\sigma_L$, the fraction of small grains $x_S = N_S/(N_S + N_L)$ and the area fraction $\phi = (N_S\sigma_S^2 + N_L\sigma_L^2)\pi/4L^2$, where $L$ is the side of the box. As shown in Fig. 1a, spheres on a substrate can be mapped onto discs owing to the introduction of a non-additivity parameter $\delta = 2\sqrt{q}(1+q) - 1$ and letting them interact at a distance smaller than $\sigma_{LS} = \frac{1}{2}(\sigma_S + \sigma_L)(1+\delta)$, where $-1 < \delta < 0$. This is the main idea underlying the effective 2D model considered in a previous numerical study focusing on elastic non-additive hard discs following dynamics at thermodynamic equilibrium[28]. This earlier study revealed that for sufficiently high-area fractions and depending on the specific $\{q, x_S\}$ combination, one can observe the self-assembly of different crystals including a 12-fold and 8-fold symmetric QC. These results are in agreement with the fact that for conservative dynamics, geometrical constraints and hard-core interactions can be minimal ingredients for the thermodynamic stability of quasi-crystalline structures[23,38]. In this work, we focus our attention on the quasi-crystalline eight-fold symmetric phase (QC8), which was observed to self-assemble more rapidly than the dodecagonal QC[28].

The collisional model we use in our simulations represents the athermal/non-equilibrium extension of the one considered in another

work[28]. It has been shown to embody dissipative and forcing mechanisms of experimental systems where spherical grains are placed on vertically vibrating horizontal substrates[39–41]. In these systems, energy is injected along the vertical direction through grain–substrate collisions and then transferred to the horizontal ones through grain–grain collisions with an efficiency that depends on the impact kinematics. In the model, the dynamics is fully 2D: there is no vibrating plate since its effect is coarse-grained out owing to the introduction of instantaneous grain–grain collisions that take into account both energy injection and dissipation. In this model, a binary collision between grains of mass $m_i$ and $m_j$ obey the following rule for the velocity ($\mathbf{v}_i$, $\mathbf{v}_j$) update:

$$\begin{aligned}\mathbf{v}_i' &= \mathbf{v}_i + \frac{m_j(1+\alpha)}{m_i+m_j}(\mathbf{v}_{ij}\cdot\hat{\boldsymbol{\sigma}}_{ij})\hat{\boldsymbol{\sigma}}_{ij} + \frac{2m_j}{m_i+m_j}\Delta\hat{\boldsymbol{\sigma}}_{ij},\\ \mathbf{v}_j' &= \mathbf{v}_j - \frac{m_i(1+\alpha)}{m_i+m_j}(\mathbf{v}_{ij}\cdot\hat{\boldsymbol{\sigma}}_{ij})\hat{\boldsymbol{\sigma}}_{ij} - \frac{2m_i}{m_i+m_j}\Delta\hat{\boldsymbol{\sigma}}_{ij},\end{aligned} \tag{1}$$

where the letters with prime symbols refer to post-collisional variables, and $\hat{\boldsymbol{\sigma}}_{ij}$ and $\mathbf{v}_{ij}$ are the unit vectors joining particles $i$ and $j$ and the relative velocity between them, respectively. The parameter $\alpha$ is the coefficient of restitution that embodies—for $0 \le \alpha < 1$—the dissipative nature of the collision. The last term in equation (1), is responsible—via parameter $\Delta$—for the velocity gain arising from the non-planar collisions that are coarse-grained out in the effective 2D description (Supplementary Information provides a more detailed explanation). By computing the energy change in a collision[39], it is possible to see that depending on the impact kinematics, one can have conditions in which the total energy decreases or increases. In this simple granular model, the limit to the equilibrium conservation case is recovered by setting $\alpha = 1$ and $\Delta = 0$.

A granular system cannot attain thermodynamic equilibrium but it can reach a non-equilibrium steady state owing to a balance between the injected and dissipated energy. Nevertheless, one can often identify a conservative system with the same geometrical properties and consider it as an equilibrium counterpart. In this perspective, non-additive hard discs in the conservative limit ($\alpha = 1$ and $\Delta = 0$) represent the equilibrium version of our granular system. Of course, given the dissipative/athermal nature of the dynamics, one cannot expect theoretical or numerical predictions for the equilibrium counterpart to hold in the granular case. However, in some specific conditions, vibrated granular materials have been shown to exhibit an equilibrium-like phenomenology, such as in the case of tracer diffusion in granular gases[42,43] or hexagonal crystal formation in monodisperse granular layers vibrated on a substrate[33,34,37]. The latter phenomenon is particularly relevant for our study since many aspects of the equivalent elastic hard-sphere crystallization have been observed even in the liquid–solid granular phase transition. The main challenging aspect for the observation of an equilibrium-like behaviour in our system is given by size polydispersity because it usually triggers non-equilibrium effects in vibrated granular materials. Size segregation[35,44–46] and violation of energy equipartition[47] are two examples of that. Thus, an important question underlying the approach we propose is the following: can we tune the non-equilibrium parameters that are related to the forcing/dissipative mechanisms of the granular system, such that the system self-assembles into quasi-crystalline structures that have been observed in the equilibrium counterpart?

Results obtained through event-driven molecular dynamics (EDMD) simulations of the model described by equation (1) are reported in Fig. 1a. Here we show the last snapshot of a simulation and the associated scattering pattern computed from the large-grain positions. The final self-assembled structure exhibits no periodic order, but the scattering peaks reveal an underlying eight-fold symmetry. This particular symmetry is forbidden by ordinary crystallographic order based on the repeated translations of a single unit cell. Indeed, in our system, the final structure can be decomposed into a combination of three different tiles, each one appearing with different orientations. In Fig. 1a, we also highlight how small and large grains combine to form such tiles: we have (1) small squares made of four large grains surrounding one small grain, (2) isosceles triangles made of three large grains surrounding one small grain and (3) large squares made of four large grains surrounding a square of small grains. The sides of the tiles coincide with bonds between large-grain nearest neighbours and we can identify long and short bonds. The former outlines large square sides and triangle legs, and the latter forms small square sides and triangle bases. In addition to the scattering pattern, another piece of evidence of the eight-fold symmetry is given by the histogram of bond orientations over the entire system (Fig. 1b). Here we can clearly see that short and long bonds are not uniformly distributed but are aligned along eight specific directions. These dominant directions are spontaneously selected among a continuum since the periodic boundary conditions do not impose preferred orientations. Within a specific eight-fold set of bond directions, small and large square tiles can only appear with two specific orientations, whereas triangle tiles can lay along eight ones. One can then classify all the tiles in the system (Methods) (Fig. 1c) and reconstruct the overall tiling of the plane (Fig. 1a, bottom left). The observed square–triangle tiling can aperiodically cover an infinite plane with long-range eight-fold orientational order. What we observe in our simulations is a finite portion of such an infinite QC: the fact that tiles with the same form but with different orientations cover a similar area fraction is coherent with this picture[28]. Additional EDMD simulations varying the geometrical parameters $\{\phi, x_s, q\}$ and non-equilibrium ones $\{\alpha, \Delta\}$, as well as considering different system sizes, confirmed the robustness of QC8 formation for this model (Supplementary Information).

We now turn our attention to the experimental realization. Our setup consists of non-magnetic steel spherical grains confined in a quasi-2D square container (height $h$ and width $L \gg h$), which is vertically vibrated by an electrodynamic shaker following a signal $z_p(t)$. The evolution of the system is followed by a camera that allows to detect the horizontal position of the grains ($x$–$y$ coordinates) as a function of time. The relevant set of explored geometrical parameters $\{q, x_s, \phi\}$ for the experiments is chosen close to those used in the simulation model. The realistic system eventually attains a non-equilibrium steady state whose dynamical properties sensitively depend on the driving force. To tune this, we performed preliminary numerical simulations of the setup implemented through the discrete element method (DEM)[48,49]. Such simulations implement granular dynamics by means of accurate contact models that allow for studying in silico prototypes of a realistic setup (Supplementary Information). From this analysis and subsequent experimental tests (Supplementary Information), we found that to observe QC8 self-assembly, one generally needs sufficiently strong vibrations to allow for an efficient vertical-to-horizontal energy transfer but not so strong that grains pile up on each other (which alters the effective 2D packing fraction of the system).

For suitable choices of driving parameters, our experimental system indeed spontaneously forms the eight-fold QC. The dynamics of this process is shown in Fig. 2a (Supplementary Video 1), where we plot the occupied area fraction as a function of time for three different groups of tile: the ones oriented according to the specific eight-fold set of directions, which dominate at the end of the experiment (green), misaligned tiles (yellow) and defects (grey). These results are obtained from a seven-day-long experiment with sinusoidal vibrations and quantify the two distinct processes contributing to the QC8 self-assembly: single tile formation and tile orientational ordering. We note that both aligned and misaligned tiles monotonously increase at very short times. After that, their evolution becomes non-monotonous: aligned tiles exhibit an increase interrupted by sudden drops, whereas misaligned tiles exhibit a decrease interrupted by sudden growths. Both of them eventually reach a final plateau. Such a behaviour reveals that once the tiles are formed and locally ordered, they still need substantial

https://doi.org/10.1038/s41567-023-02364-1

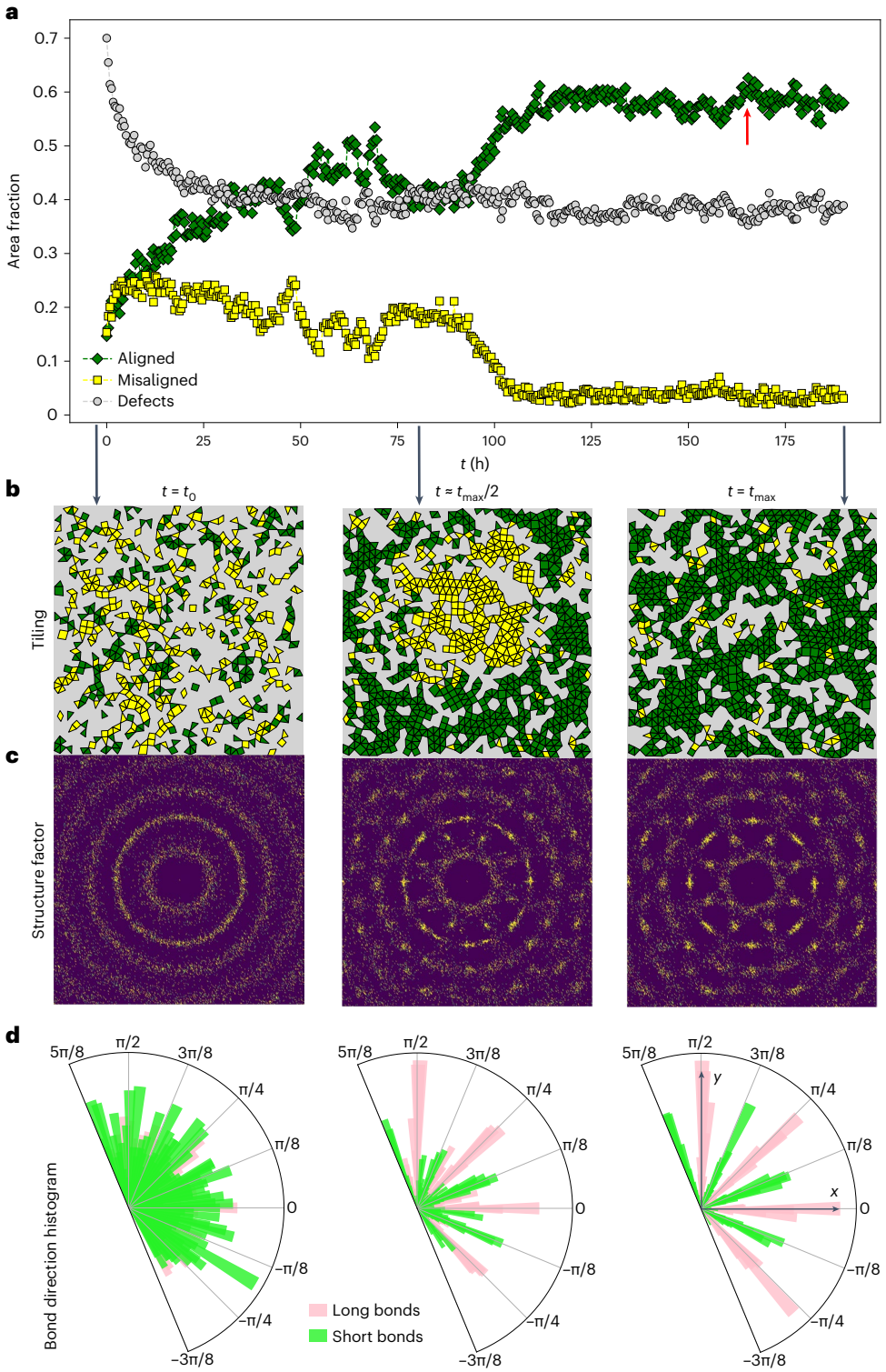


**Fig. 2 | Experimental results: time evolution.** The following parameters are considered: $\{q, x_s, \phi\} = \{0.5, 0.675, 0.848\}$, $N_S + N_L = 3{,}840$, $\sigma_L = 2.381$ mm, $z_p(t) = A\sin(2\pi ft)$, where $A = 22$ μm and $f = 120$ Hz. Data from real-time measurements during QC8 formation (Supplementary Video 1). **a**, Area fraction of tiles correctly aligned according to the dominant orientational order, misaligned tiles and defects. The error bars due to possibly undetected grains are smaller than the symbol sizes. The red arrow indicates the time of the configuration shown in Fig. 3. **b**–**d**, Reconstructed tiling (**b**), structure factor (**c**) and bond orientation histogram (**d**) for early, intermediate and late times. The yellow tiles are misaligned with the final long-range order, and the green ones are in agreement with it. We note that the latter have long bonds laying on the $x$–$y$ axis (Supplementary Video 1).

rearrangements to form larger quasi-crystalline domains, and this makes the QC formation extremely slow.

From the evolution of reconstructed tilings (Fig. 2b), we observe that QC8 with the dominant eight-fold symmetry is growing from the boundaries towards the bulk. During this process, it is possible to observe the coexistence between different misaligned QC domains ($t \approx t_{max}/2$). In Fig. 2c, we also show the evolution of the structure factor: the initial configuration shows the typical rings of a liquid-like

https://doi.org/10.1038/s41567-023-02364-1

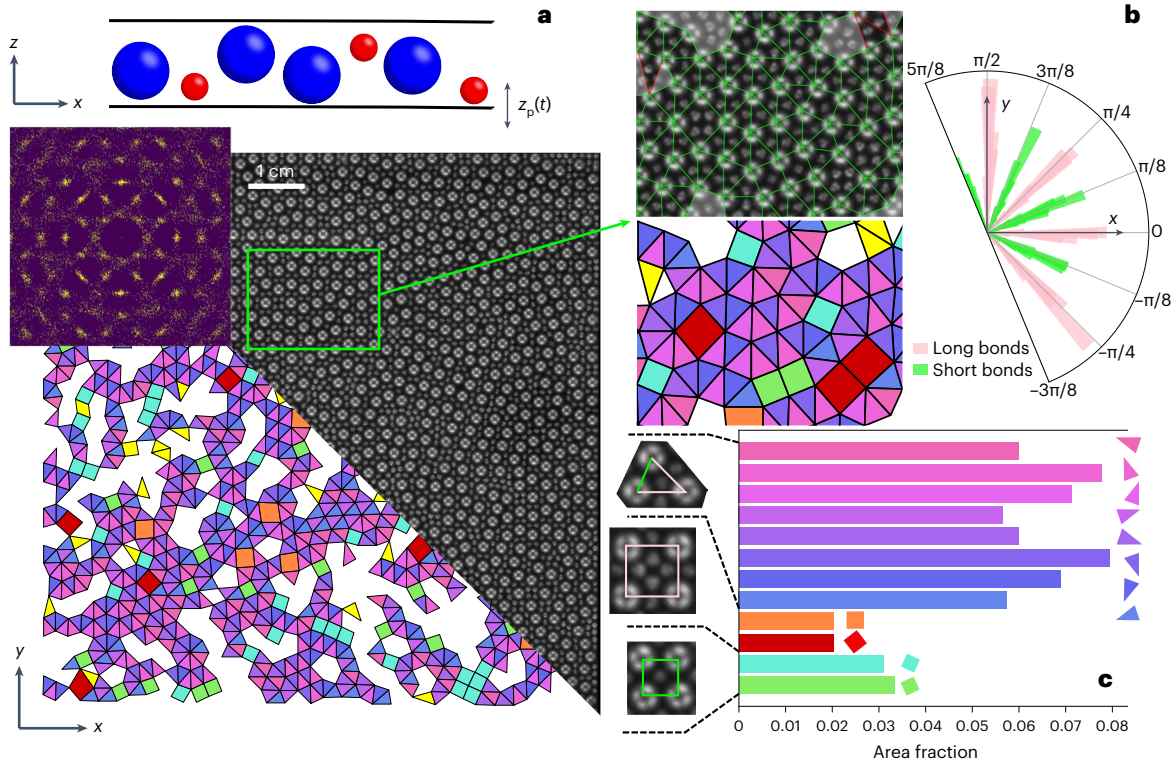


**Fig. 3 | Experimental results: self-assembled structure. a**, Configuration, structure factor and reconstructed tiling obtained after ~170 h of the experimental run (shown in Fig. 2). The specific snapshot shown here is the one with the highest QC8 area fraction (Fig. 2, red arrow). We also show a sketch of the $x$–$z$ projection of the setup and a comparison between real-space tiling and the reconstructed one in a zoomed-in view of the region on the sample. **b**, Bond orientation histogram. **c**, Tile area fraction histogram with a snapshot of single granular tiles forming the QC.

structure, the middle one exhibits blurred peaks originating from the coexistence of multiply oriented QC domains and the last one presents sharper peaks highlighting the long-range order according to a dominant set of eight directions. Finally, from the evolution of the bond orientation histogram (Fig. 2c), we can see that the most favoured set of orientations is the one with large tile sides aligned with the hard walls. Repetitions of the experiment revealed that this is a reproducible feature. Indeed, an important difference with respect to the numerical case discussed above is represented by the hard horizontal walls that break the orientational symmetry. The enforced grain alignment at the $x$–$y$ boundaries favours two specific sets of eight-fold symmetric directions: one with short bonds and one with long bonds aligned with the walls. The dominance of the latter can be explained considering that the forming quasi-crystalline structure requires much more long bonds than short ones.

An interesting picture emerges: tiles of the desired shapes form very rapidly, probably as a consequence of their efficient local packing. However, global alignment requires much more collective rearrangements that appear to be rare events. It is important to point out that the real-time measurements of forming quasi-crystalline structures are extremely rare in experiments. Generally, the techniques used for QC self-assembly (for example, the evaporation of nanoparticle solutions) are not compatible with the observation of dynamics during the ordering process but only allows to analyse the final structure. The experimental study of system configurations over time is then another important novelty of macroscopic QCs since it can shed light on the unexplored dynamical properties of QC self-assembly.

In Fig. 3a, we show the spatial configuration, related scattering pattern and reconstructed tiling obtained from the experimental configuration with the largest quasi-crystalline area fraction (Fig. 2a, red arrow). On the right side of the same figure, we report the histograms of bond orientation (Fig. 2b) and tile area fraction (Fig. 2c). We note that the key properties of the quasi-crystalline structure observed in EDMD simulations are also found in the experiment: we have the same eight-fold long-range orientational order, confirmed by the scattering intensity, and the same square–triangle tiling. By comparing Figs. 1 and 3, we realize that the main difference between the EDMD simulations and experiments is the presence of larger defects in the latter. It is difficult to pin down the origin of this difference as the $z$-to-$x$–$y$ energy transfer mechanism of the real experimental model depends—in a highly non-trivial way—on the dissipative properties of the materials and plate roughness, whereas energy injection in the EDMD simulations is fully described by a simple collision rule that depends only on two parameters. We argue that larger defects are also the reason why we observe lower large-square-area fraction in the experiment with respect to EDMD (compare Figs. 1c and 3c). In fact, large squares are favoured by a large number of small grains[28], but many of them are stuck in defects that mainly appear as clusters of small grains. Despite these differences, we find it remarkable that the EDMD simulations effectively capture the essence of non-equilibrium self-assembly. Moreover, this computational scheme is considerably simpler compared with DEM simulations and could serve as a vital tool in further explorations of this phenomenon.

To test the robustness and reproducibility of the discussed results, we repeated the experiment for different initial random configurations, different drivings (sawtooth vibrations) and slightly shifted state points. As reported in the Supplementary Information, the emergence of a quasi-crystalline order proved to be a fairly robust feature of this granular system.

More than 40 years ago, the QC self-assembly paradigm emerged in purely atomistic systems, but was later extended to the nanometric and micrometric scales typical of soft matter. Here we have shown

that this idea can be extended to much larger length scales in vibrofluidized granular systems. Our study reports the first observation of quasi-crystalline order in a physical system undergoing athermal dynamics in the visible scale, where the real-time measurements of system configuration can be performed during the self-assembly process. The passage from the micrometre to the millimetre scale is not a trivial one, since in the latter, the grains do not undergo thermal agitation. In a seminal work[50], entropic reasoning was employed to elucidate the behaviour of jammed granular systems (or 'powders' as termed in that study). However, such an approach hinges on the presumption of a jammed state, an assumption not applicable to our vibrofluidized systems. An apt theoretical framework should ideally extend the equilibrium vibrational entropy, which is instrumental in stabilizing the QC[38], to non-equilibrium conditions, perhaps drawing on kinetic theories. Despite this fundamental difference, a quasi-crystalline order emerges in the same conditions as predicted at equilibrium, something that could not be trivially expected.

## Online content

Any methods, additional references, Nature Portfolio reporting summaries, source data, extended data, supplementary information, acknowledgements, peer review information; details of author contributions and competing interests; and statements of data and code availability are available at https://doi.org/10.1038/s41567-023-02364-1.

## References


1. Shechtman, D. & Blech, I. A. The microstructure of rapidly solidified $Al_6Mn$. *Metall. Trans. A* **16**, 1005 (1985).
2. Levine, D. & Steinhardt, P. J. Quasicrystals: a new class of ordered structures. *Phys. Rev. Lett.* **53**, 2477 (1984).
3. Report of the Executive Committee for 1991. *Acta Cryst.* **A48**, 922–946 (1992).
4. DiVincenzo, D. & Steinhardt, P. *Quasicrystals: The State of the Art* (World Scientific, 1999).
5. Ranganathan, S. & Chattopadhyay, K. Quasicrystals. *Annu. Rev. Mater. Sci.* **21**, 437 (1991).
6. Bindi, L., Steinhardt, P. J., Yao, N. & Lu, P. J. Natural quasicrystals. *Science* **324**, 1306 (2009).
7. Bindi, L. et al. Evidence for the extraterrestrial origin of a natural quasicrystal. *Proc. Natl Acad. Sci. USA* **109**, 1396 (2012).
8. Hayashida, K., Dotera, T., Takano, A. & Matsushita, Y. Polymeric quasicrystal: mesoscopic quasicrystalline tiling in ABC star polymers. *Phys. Rev. Lett.* **98**, 195502 (2007).
9. Barkan, K., Diamant, H. & Lifshitz, R. Stability of quasicrystals composed of soft isotropic particles. *Phys. Rev. B* **83**, 172201 (2011).
10. Talapin, D. V. et al. Quasicrystalline order in self-assembled binary nanoparticle superlattices. *Nature* **461**, 964 (2009).
11. Takano, A. et al. A mesoscopic Archimedean tiling having a new complexity in an ABC star polymer. *J. Polym. Sci. B Polym. Phys.* **43**, 2427 (2005).
12. Zeng, X. et al. Supramolecular dendritic liquid quasicrystals. *Nature* **428**, 157 (2004).
13. Zhang, J. & Bates, F. S. Dodecagonal quasicrystalline morphology in a poly(styrene-*b*-isoprene-*b*-styrene-*b*-ethylene oxide) tetrablock terpolymer. *J. Am. Chem. Soc.* **134**, 7636 (2012).
14. Lifshitz, R. & Diamant, H. Soft quasicrystals—why are they stable?. *Philos. Mag.* **87**, 3021 (2007).
15. Lee, S., Bluemle, M. J. & Bates, F. S. Discovery of a Frank-Kasper σ phase in sphere-forming block copolymer melts. *Science* **330**, 349 (2010).
16. Wasio, N. A. et al. Self-assembly of hydrogen-bonded two-dimensional quasicrystals. *Nature* **507**, 86 (2014).
17. Förster, S., Meinel, K., Hammer, R., Trautmann, M. & Widdra, W. Quasicrystalline structure formation in a classical crystalline thin-film system. *Nature* **502**, 215 (2013).
18. Jin, C. et al. Band gap and wave guiding effect in a quasiperiodic photonic crystal. *Appl. Phys. Lett.* **75**, 1848 (1999).
19. Zoorob, M. E., Charlton, M. D. B., Parker, G. J., Baumberg, J. J. & Netti, M. C. Complete photonic bandgaps in 12-fold symmetric quasicrystals. *Nature* **404**, 740 (2000).
20. Liu, Y. et al. Expanding quasiperiodicity in soft matter: supramolecular decagonal quasicrystals by binary giant molecule blends. *Proc. Natl Acad. Sci. USA* **119**, e2115304119 (2022).
21. Fischer, S. et al. Colloidal quasicrystals with 12-fold and 18-fold diffraction symmetry. *Proc. Natl Acad. Sci. USA* **108**, 1810 (2011).
22. Xiao, C., Fujita, N., Miyasaka, K., Sakamoto, Y. & Terasaki, O. Dodecagonal tiling in mesoporous silica. *Nature* **487**, 349 (2012).
23. Haji-Akbari, A. et al. Disordered, quasicrystalline and crystalline phases of densely packed tetrahedra. *Nature* **462**, 773 (2009).
24. Noya, E. G., Wong, C. K., Llombart, P. & Doye, J. P. K. How to design an icosahedral quasicrystal through directional bonding. *Nature* **596**, 367 (2021).
25. Widom, M., Strandburg, K. J. & Swendsen, R. H. Quasicrystal equilibrium state. *Phys. Rev. Lett.* **58**, 706 (1987).
26. Dotera, T., Oshiro, T. & Ziherl, P. Mosaic two-lengthscale quasicrystals. *Nature* **506**, 208 (2014).
27. Malescio, G. & Sciortino, F. Self-assembly of quasicrystals and their approximants in fluids with bounded repulsive core and competing interactions. *J. Mol. Liq.* **349**, 118209 (2022).
28. Fayen, E., Impéror-Clerc, M., Filion, L., Foffi, G. & Smallenburg, F. Self-assembly of dodecagonal and octagonal quasicrystals in hard spheres on a plane. *Soft Matter* **19**, 2654 (2023).
29. Fayen, E., Jagannathan, A., Foffi, G. & Smallenburg, F. Infinite-pressure phase diagram of binary mixtures of (non) additive hard disks. *J. Chem. Phys.* **152**, 204901 (2020).
30. Jaeger, H. M., Nagel, S. R. & Behringer, R. P. Granular solids, liquids, and gases. *Rev. Mod. Phys.* **68**, 1259 (1996).
31. Andreotti, B., Forterre, Y. & Pouliquen, O. *Granular Media: Between Fluid and Solid* (Cambridge Univ. Press, 2013).
32. Eshuis, P., van der Weele, K., van der Meer, D., Bos, R. & Lohse, D. Phase diagram of vertically shaken granular matter. *Phys. Fluids* **19**, 123301 (2007).
33. Olafsen, J. S. & Urbach, J. S. Clustering, order, and collapse in a driven granular monolayer. *Phys. Rev. Lett.* **81**, 4369 (1998).
34. Reis, P. M., Ingale, R. A. & Shattuck, M. D. Crystallization of a quasi-two-dimensional granular fluid. *Phys. Rev. Lett.* **96**, 258001 (2006).
35. Aranson, I. S. & Tsimring, L. S. Patterns and collective behavior in granular media: theoretical concepts. *Rev. Mod. Phys.* **78**, 641 (2006).
36. Panaitescu, A., Reddy, K. A. & Kudrolli, A. Nucleation and crystal growth in sheared granular sphere packings. *Phys. Rev. Lett.* **108**, 108001 (2012).
37. Komatsu, Y. & Tanaka, H. Roles of energy dissipation in a liquid-solid transition of out-of-equilibrium systems. *Phys. Rev. X* **5**, 031025 (2015).
38. Fayen, E., Filion, L., Foffi, G. & Smallenburg, F. A hard-sphere quasicrystal stabilized by configurational entropy. Preprint at https://arxiv.org/abs/2306.03549 (2023).
39. Brito, R., Risso, D. & Soto, R. Hydrodynamic modes in a confined granular fluid. *Phys. Rev. E* **87**, 022209 (2013).
40. Brito, R., Soto, R. & Garzó, V. Energy nonequipartition in a collisional model of a confined quasi-two-dimensional granular mixture. *Phys. Rev. E* **102**, 052904 (2020).

41. Garzó, V., Brito, R. & Soto, R. Navier–Stokes transport coefficients for a model of a confined quasi-two-dimensional granular binary mixture. *Phys. Fluids* **33**, 023310 (2021).
42. D'Anna, G., Mayor, P., Barrat, A., Loreto, V. & Nori, F. Observing Brownian motion in vibration-fluidized granular matter. *Nature* **424**, 909 (2003).
43. Sarracino, A., Villamaina, D., Costantini, G. & Puglisi, A. Granular Brownian motion. *J. Stat. Mech.* **04013**, P04013 (2010).
44. Aumaitre, S., Kruelle, C. A. & Rehberg, I. Segregation in granular matter under horizontal swirling excitation. *Phys. Rev. E* **64**, 041305 (2001).
45. Baldassarri, A., Puglisi, A. & Sarracino, A. Coarsening in granular systems. *C. R. Phys.* **16**, 291 (2015).
46. Kudrolli, A. Size separation in vibrated granular matter. *Rep. Prog. Phys.* **67**, 209 (2004).
47. Feitosa, K. & Menon, N. Breakdown of energy equipartition in a 2D binary vibrated granular gas. *Phys. Rev. Lett.* **88**, 198301 (2002).
48. Cundall, P. A. & Strack, O. D. L. A discrete numerical model for granular assemblies. *Géotechnique* **29**, 47 (1979).
49. Pöschel, T. & Schwager, T. *Computational Granular Dynamics* (Springer, 2005).
50. Edwards, S. & Oakeshott, R. Theory of powders. *Phys. A: Stat. Mech. Appl.* **157**, 1080 (1989).

# Methods

## Experimental setup and protocol

Our experimental setup (Supplementary Fig. 1 shows a schematic) consists of a binary mixture of non-magnetic stainless steel grains (Marteau & Lemarié) lying on a square anodized aluminium plate (1 cm thick), which is vertically vibrated by an electrodynamic shaker (Brüel & Kjær, LDS V400). The plate is attached to the shaker through an additional aluminium support. Four aluminium spacers are screwed on the plate to confine the motion of the grains in a square area of side $L = 10$ cm through lateral walls of height $h = 6$ mm. Other relevant dimensions are the small-grain diameter $\sigma_S = 1.200$ mm, large-grain diameter $\sigma_L = 2.381$ mm, lateral side of the plate $L_p = 20$ cm. The granular system is confined from above by a glass cover (2 mm thick); therefore, the snapshots of the horizontal spatial configuration can be acquired with a high-resolution (5 MP) camera (Basler a2A2590) placed above the setup. The camera is equipped with a lens (Basler C125-1218-5M-P) having a fixed focal length of 12.0 mm. The total mass of the quasi-2D cell (consisting of plate, additional support, spacers and glass cover) is $M_c = 2{,}250$ g, whereas the total mass of the granular sample is $M_s$ between 88 and 90 g depending on its composition and packing fraction. To ease the imaging of the grain, four light panels are placed around the apparatus. The measurements of the plate acceleration are made possible by a one-axis accelerometer (Brüel & Kjær, Type 4534-B-001) that can be rigidly joined to its bottom side. The base of the apparatus is held up by three levelling feet, which allow for horizontal adjustment.

During a preliminary analysis, we found that the self-assembly process is very sensitive to small inclinations of the quasi-2D box with respect to the horizontal. Indeed, when gravity acts on the grains in a direction that is not perpendicular to the plate surface, we could observe both particle size segregation and heterogeneous mobility. It was then important to calibrate the setup by tuning the plate surface to be as horizontal as possible (Supplementary Information shows our protocol). After this calibration, we prepare the granular sample with the desired $q$, $x_S$ and $\phi$; pour it into the quasi-2D cell; and randomize the initial configuration with highly energetic shaking. We then impose the previously identified optimal driving conditions (sawtooth or sinusoidal; Supplementary Information) and start the acquisition of the horizontal snapshots. We specify that for the range of driving parameters we explored, the grains do not collide with the glass cover except when we perform the initial randomization. We usually acquire one snapshot every 30 s. The DEM simulations were also used to characterize the systems and find the optimal driving conditions (Supplementary Information).

## Image processing

All the experimental data on granular self-assembly discussed in this work have been extracted from the images of the $x$–$y$ system projection acquired with the high-resolution camera placed on top of the setup. To detect the $x$–$y$ coordinates of the grains, we used the 'match template' function of the scikit-image package for Python 3.10.12[51] implementing a zero-mean normalized cross-correlation. This function finds the instances of a given template in an image through the normalized cross-correlation. Using the cropped images of one small and one large grain as the template, we were able to efficiently detect the particle positions in the system (Supplementary Fig. 1).

## Driving signals and acceleration measurements

In the experiment, we consider two different driving conditions: sinusoidal and sawtooth vibrations. Here we explain how we impose them onto the granular system; in the Supplementary Information, we compare the self-assembled structures obtained through the two methods.

The electric signal $s(t)$ is produced by a wave generator (Keysight 33220A). It is first sent to an amplifier (Brüel & Kjær, LDS LPA600) and subsequently to the electrodynamic shaker, which converts current into a force that is proportional to $s(t)$ applied to the quasi-2D box by means of an electromagnet. We measure the resulting imposed vertical acceleration $\ddot{z}_p(t) = a_{max}s(t)$ with the accelerometer rigidly joined to the vibrating box. The values measured from this sensor can be read (in voltage units) by a multimeter (Keithley 199 SYSTEM DMM/SCANNER) or an oscilloscope (Tektronix TBS 1052B-EDU) and then converted into acceleration units with the conversion factors found in the documentation (10.14 mV ms$^{-2}$ to 99.44 mV g$^{-1}$). In the case of sinusoidal driving, we can easily obtain the imposed displacement (which is still sinusoidal) $z_p(t) = A\sin(2\pi ft)$, where $A = a_{max}/(2\pi f)^2$ and $f$ coincides with the frequency chosen for $s(t)$. Throughout the paper, we characterize sinusoidal driving by the pair of parameters $f$ and $A$, where $A$ is calculated from $a_{max}$ as measured from the acceleration $\ddot{z}_p(t)$ of the quasi-2D box without the granular sample. Note that, in practice, the amplitude of the box with beads is expected to be lower due to the additional weight, but this amplitude is significantly harder to measure due to the fact that bead collisions with the plate add noise to the signal of the accelerometer. However, we expect this difference to be very small since the total mass of the granular sample is much smaller than the one of the quasi-2D cell ($M_s/M_c \approx 0.04$). To characterize a sawtooth signal, we instead rely on $a_{max}$ and $f$, which are directly measured from $\ddot{z}_p(t) = a_{max}[2(ft - 1/2) \bmod 1]$ with the empty cell.

In calibrating the experimental setup, we conducted multiple measurements with the accelerometer oriented along $z$. In-plane acceleration measurements are made possible by attaching the same sensor to the setup but oriented along $x$ and $y$. We performed such an analysis for both sinusoidal and sawtooth vibrations and compared it with the results obtained for the $z$ axis. We have done that with the same quasi-2D cell used in the experiment but without the granular sample. We found that for sinusoidal vibrations, the root mean squared values of the in-plane accelerations are always a very small fraction of the vertical one, $a_z$. Moreover, their values are of the order of the acceleration we measure when no vibration is imposed on the setup. In other words, horizontal accelerations are almost indistinguishable from the background noise of the instrumentation. Things are different in the case of sawtooth driving for which we measured accelerations of the same order of magnitude along the three directions. From this analysis, we can conclude that our experiments have been conducted in the presence of pure vertical driving but also in cases with measurable in-plane accelerations (possibly due to the vibrational modes of the plate). The fact that the QC8 self-assembly has been observed in both cases (main text and Supplementary Information) is a further test for the robustness of our results.

## EDMD simulations

EDMD is used to solve the dynamics presented in equation (1). EDMD is based on the assumption that at each instant, at most one contact between two particles of infinitesimal duration occurs throughout the system. This allows to save computational resources since time is not discretized and the integration of motion jumps from a collision to the consecutive one (in between, there are just predictable free flights). The simulations we performed are based on an optimized algorithm for EDMD for hard-sphere systems[52] (Supplementary Information provides more details and additional results).

## Tiling analysis

The reconstructed tilings (main text and Supplementary Information) are obtained by extracting the bond network of large grains and identifying cycles in it after removing the crossing bonds. The latter arise since—to identify both short and long bonds—we use a nearest-neighbour threshold of $1.8\sigma_L$, which is larger than the small-square diagonal $\sqrt{2}\sigma_L$. Each cycle can then be categorized as a polygon compatible with the eight-fold square–triangle tiling (small squares, large squares and triangles) or as a defect. Then, among the tiles compatible with the QC8 structure, we select the ones that are correctly aligned (with a tolerance

of ±π/32) with the set of eight directions that dominate at the end of the experiment/simulation. The remaining tiles are either misaligned from that set of orientations or ambiguously oriented. The latter condition occurs when, because of slight deformations, different bonds in a tile are compatible with different overall orientations of the reference polygon. The classification of tiles is performed as follows. We start by considering the reference set of eight versors characterizing the long-range order at the end of the experiment/simulation. After that, in each snapshot, we measure the orientation of long and short bonds and find the relative closest versors of the aforementioned set. Then, for bonds belonging to isosceles triangles (whose orientation is identified by the versor connecting the middle point of the base and the vertex where the two legs meet), we proceed in this way: first, we consider the orientation of the short bond and determine the two overall triangle orientations that are compatible with it. Then, we independently determine the orientation of the tile from the ones of the two long bonds. If this coincides with one of the two identified with the short bond and the angular distance between the measured orientation and the closest one in the reference set is below a given threshold (±π/32), then we classify the triangle oriented along it. If the angular distance from the versor in the reference set is larger than the threshold, then the triangle is considered misaligned with respect to the final long-range orientational order. However, if the orientation determined by the two long bonds does not match one of the two identified by the short one, the tile is classified as ambiguously oriented. For both large and small squares, the orientation of a single side is enough to determine if the overall orientation of the tile is compatible with one of the two that appear in the dominant aperiodic tiling at the end of the experiment/simulation. So, if at least three sides of a square are compatible (within ±π/32) with the same overall orientation of the final tiling, we classify the square oriented along it. Then, we consider misaligned squares as the ones that do not match the threshold and ambiguously oriented squares as the ones in which there are less than three sides compatible with the same overall orientation.

## Data availability

Raw datasets generated during this study are available from the corresponding author on reasonable request. Source data are provided with this paper.

## Code availability

The code of the EDMD simulations is available via GitHub at https://github.com/Syrocco/EDMD-QC8. The DEM simulations are implemented through the LAMMPS package available at https://www.lammps.org/.

## References

51. S. van der Walt, J. L. Schönberger, J. Nunez-Iglesias, F. Boulogne, J. D. Warner, N. Yager, E. Gouillart, T. Yu, and the scikit-image contributors. Scikit-image: image processing in Python. *Peer J.* **2**, e453 (2014).
52. Smallenburg, F. Efficient event-driven simulations of hard spheres. *Eur Phys. J. E* **45**, 22 (2022).

## Acknowledgements

We thank A. Puglisi and A. Gnoli for their invaluable help in setting up this project and for their comments on the manuscript. We also thank M. Impéror-Clerc, L. Filion, A. Jagannathan and F. Sciortino for carefully reading and commenting on our paper and S. Cabaret for the design of the quasi-2D cell. This work has been done with the support of Investissements d'Avenir of LabEx PALM (grant no. ANR-10-LABX-0039-PALM) and of the Agence Nationale de la Recherche (ANR), grant ANR-18-CE09-0025.

## Author contributions

G.F. and F.S. conceived the work and supervised the research. A.P, F.R., F.B. and G.F. designed the experiment. A.P. performed the experimental research and analysed the experimental data. A.P., E.F. and R.M. designed the simulations. A.P. and R.M. performed the simulations and analysed the data from the simulations. A.P., F.S. and G.F. wrote the paper. All authors reviewed and commented on the paper and the Supplementary Information.

## Competing interests

The authors declare no competing interests.

## Additional information

**Supplementary information** The online version contains supplementary material available at https://doi.org/10.1038/s41567-023-02364-1.

**Correspondence and requests for materials** should be addressed to A. Plati or G. Foffi.

**Peer review information** *Nature Physics* thanks Joshua Dijksman, Eva Noya and the other, anonymous, reviewer(s) for their contribution to the peer review of this work.